UNIVERSITY OF ILLINOIS

May 29 19 86

THIS IS TO CERTIFY THAT THE THESIS PREPARED UNDER MY SUPERVISION BY

BENJAMIN CARL WIEGAND

ENTITLED HIGH PRESSURE STUDY OF HYDROLYSIS OF TMOS AND

THE SOLUBILITY OF ANTHRACENE IN SUPERCRITICAL CO_2

IS APPROVED BY ME AS FULFILLING THIS PART OF THE REQUIREMENTS FOR THE

DEGREE OF BACHELOR OF SCIENCES IN CHEMISTRY

Instructor in Charge

APPROVED:

HEAD OF DEPARTMENT OF Chemistry

O-1364

HIGH PRESSURE STUDY OF HYDROLYSIS OF TMOS

AND

THE SOLUBILITY OF ANTHRACENE IN SUPERCRITICAL CO_2

BY

BENJAMIN CARL WIEGAND

THESIS

for the

DEGREE OF BACHELOR OF SCIENCE

IN

CHEMISTRY

College of Liberal Arts and Sciences

University of Illinois

Urbana, Illinois

1986

Acknowledgments

I would like to express my appreciation to Dr. Jiri Jonas for giving me the opportunity to do my research and most of all for his helpful comments and suggestions along the way. Thanks also go to Xiaomin Song for help in some of the Raman work. I also wish to thank the National Science Foundation for their support. Finally, I wish to thank Dr. T. W. Zerda for all of his aid during the last year, his suggestions and ideas, his patience with me and his guidance, without which this research would not have been accomplished.

Table of Contents

Due to recent progress in experimental techniques, one can witness a transition from a purely empirical research approach to atomic and molecular level studies of complex systems. This thesis addresses problems relevant to two chemical areas of industrial interest: supercritical fluid extraction and sol-gel process for preparing glasses or ceramics. The thesis is divided into three main parts. The first part deals with the FTIR study of anthracene in compressed supercritical CO_2. The pressure effects on hydrolysis of tetramethoxysilane are discussed in the second part. The attempt for random-walk simulation of particle growth concludes this study.

Chapter I

FTIR Measurement of Anthracene in Supercritical CO_2

A. Introduction

During the past few years solvent extraction with supercritical fluids has become an important technological process. It has been used in decaffeinating coffee beans [1], regenerating activated carbon [2], deasphalting petroleum [3], separating organic chemicals from water [4], separating of a mixture of aromatic isomers [5] and in many other processes [6]. In these extraction processes the effectiveness of the solvent is characterized by solubility data of the solid. So far, most solubilities have been measured using flow techniques [7,8]. Two new methods have recently been developed in this laboratory, one involving NMR high pressure experiments [9], and another using infrared absorption measurements. FTIR is especially well suited to determine solubilities in supercritical fluids because aromatic molecules have numerous IR active modes, and it is easy to find one or more characteristic bands well isolated from the solvent bands. The intensity of the solute band can be accurately determined, and from the Lambert-Beer law concentrations of solids can be found at various temperatures and pressures.

In this paper, we describe the FTIR technique and then present the results for the CO_2 - anthracene system. Solubility data for anthracene are scarce; until now only two studies have been reported. Rossling and Frank [10] used UV absorption measurements and from peak intensities

found solubilities of anthracene in numerous fluids (CO_2, NH_3, H_2O, CH_4, CHF_3 and others) at temperatures varying from 20°C to 200°C and pressures up to 2000 bar. Kwiatkowski et al. [11] used the flow technique and limited their study of anthracene in CO_2 to 40°C and pressures ranging from 100 to 200 bar. Our results are compared to those reported in Refs. 10 and 11 and also presented in the form of the enhancement factor. This factor measures the extent to which a solvent enhances the solute concentration C as compared with the vapor concentration C^o in equilibrium with the solid phase without the solvent.

B. Experiment

The concentration of a solute in a solution can be found from the intensity of the IR absorption band. Absorbance is given as $A = \ln$, where I_o is the background and $I(\nu)$ is the intensity of the vibrational peak at frequency ν, and according to the Lambert-Beer law it is proportional to

$$A(\nu) = \varepsilon(\nu)\, C\, d \quad . \qquad (1)$$

C is the concentration of the sample in solution, d is the optical path length and $\varepsilon(\nu)$ is the absorption coefficient characteristic for the vibration band. For this study we concentrated on the C-H stretching vibration modes of anthracene located at about 3060 cm^{-1}. The molar absorption coefficient at the maximum of the 3060 cm^{-1} band was found to be $\varepsilon = 180$ l cm^{-1} mol^{-1} ± 10%. The detailed discussion of this value as well as how it has been determined is given in the next section.

All the experiments were performed using the FTIR Nicolet 9000 series spectrometer. Construction of the high pressure IR cell built of stainless steel and equipped with cylindrical saphire windows of diameter 18 mm and thickness 12 mm is based on that described in Ref. 12. The windows were mounted on stainless steel plugs using a very thin indium foil spacer (5 μm). To allow measurements with the optical path length less than 1 mm, the windows were constructed in such a way that the window cups were completely hidden and did not protrude above the window surface (see Fig. 1). The distance between the windows could be changed from 0.2 mm to 16 mm by using Bridgeman type O-rings of different length. The optical path length was determined to within + 0.03 mm.

Temperature was measured using a thermocouple located within the sample cell. Temperature was regulated by circulating fluid through the heating jacket surrounding the cell. Although the windows are located well inside the cell (Fig. 1), we found that their surface temperature was slightly lower (up to 3°C) than that of the cell. Thus, in order to prevent deposition of vapor anthracene on the cooler windows, the windows were heated by electrical coils mounted on the plugs.

Ultra pure CO_2 was purchased from Scientific Gas Product, Inc. This gas contained less than ' ppm of hydrocarbons which absorb infrared radiation at frequencies from 3010 cm^{-1} to 28[illegible] cm^{-1}, below the region where anthracene C-H bands are located. Prior to the main experiment, the absorption spectra of CO_2 were recorded at all of the studied temperatures and pressures. These spectra were later carefully subtracted from the overall band shape of anthracene - CO_2 mixtures.

Several pieces of anthracene crystals were inserted through the thermocouple opening and were placed in a shallow dent in the bottom of the cell well below the light beam. To avoid contamination with water and atmospheric gases, the system (membrane compressor, tubings, valves and the cell) was purged with CO_2 and later vacuum pumped. Spectra were recorded and stored only after the solubility equilibrium had been reached. This usually took 30 minutes, but in a few cases we waited from 8 to 12 hours to be sure that equilibrium had been reached. Pressure was determined within 0.5 bar and temperature was stabilized to better than ± 0.2°C. The densities of CO_2 at various pressures and temperatures were calculated from the fifth order polynomials found by the least square fitting routine to the density data published by Newitt et al. [13].

C. Results

The solubility data of the anthracene in carbon dioxide are listed in Table 1 (in mol l^{-1}) and Table 2 (in mole fraction), and some values are also plotted in Fig. 2. The experimental error of the A/d ratio found by repeating the measurements 3 times, each with different optical path lengths is less than 5%, but we estimate that the data in Table 1 are accurate only to within 20%. This is because of uncertainties as to the value of the molar absorption coefficient, ε. IR absorption measurements of vapor anthracene in equilibrium with the solid phase provided us with $\varepsilon = 200 \pm 20$ l cm^{-1} mol^{-1}. Because vapor concentration of anthracene is very small at room temperature [10], the calibration measurements were taken at elevated temperatures varying from 120°C to 150°C. At

these temperatures, condensation of anthracene on the windows was a serious problem so the cell 150mm long was equipped with double KBr windows. Since the ε is proportional to the transition dipole moment which is sensitive to intramolecular interactions, ε may vary with solvent. For example, we found ε of the C-H band of anthracene to be 230 + 10 ! cm^{-1} mol^{-1} and 205 + 9 1 cm^{-1} mol^{-1}, for CS_2 and CCL_4 solutions, respectively. We found our data to be in good agreement with the solubilities of anthracene in CO_2 published by Rossling and Franck [10] (as illustrated in Fig. 3) for the molar absorption coefficient ε = 180 1 cm^{-1} mol^{-1}. All the calculations of anthracene concentration in CO_2 were performed using Eq. 1 assuming ε = 180 1 cm^{-1} mol^{-1}. Since the ε may change with temperature, pressure and also with anthracene concentration in solutions, we have examined the C-H mode molar absorption coefficient of anthracene under various conditions in CCL_4 solutions. No trend has been observed because the data were scattered within the estimated 4% experimental error. Based on these observations we assumed that the ε in CO_2 solutions was constant at the pressures and temperatures studied.

Comparison of our data with other reported solubility data [11] obtained by using the flow technique is not as satisfactory. Kwiatkowski et al. [11] found concentrations of anthracene in CO_2 to be larger than those cited in this paper by about 30% (compare Table 2), and these discrepancies cannot be attributed to inaccuracies in determining the ε values. It is worth noting that the flow technique used by Kwiatkowski et al. [11] is not well suited for measurements of concentration at low solubilities on the order of 10^{-5} mole fraction, in contrast to the FTIR absorption method employed in this study.

It is useful to present the concentration data, C, in the form of enhancement factor C/C^{o}, where C^{o} is the vapor concentration in equilibrium with solid phase (C^{o} values were found in Table 2 of Ref. 10). After a steep increase the enhancement exceeds a value of 10^{5} at 40°C and 10^{4} at 95°C (compare Fig. 4). Although the absolute solubilities increase with increasing temperature the enhancement factor declines at higher temperatures. At low pressures the enhancement factor increases linearly with solvent density to about 0.9 kg/l and later a saturation is observed. A further rise of solvent density does not affect the enhancement factor. A similar observation was reported previously by Rossling and Franck [10].

In Fig. 5 we present frequency shift data for three representative temperatures. With increasing temperature and/or pressure the C-H band of anthracene shifts to higher frequency. To the best of our knowledge, this blue shift is characteristic for repulsive forces dominating in the intermolecular interactions [14,15]. This observation is limited to the C-H vibrations located in the plane of the anthracene molecule, and therefore does not preclude the possibility that attractive forces dominate the interactions between CO_2 and the π electron system of anthracene causing the increased solubility. Additional experiments focusing on frequency shifts of ring vibrations of anthracene are now in progress.

Figure Captions

Figure 1. High pressure stainless steel IR cell. 1 - cell body, 2 - plug, 3 - saphire window, 4 - Bridgeman rings, 5 - window cup, 6 -extraction ring, 7 - electrical coil, 8 - high pressure tube with connection to the cell. Thermocouple inlet is perpendicular to the section shown.

Figure 2. Solubilities of anthracene in CO_2 at different densities. O: 0.294 kg/l, Δ: 0.643 kg/l, □: 0.803 kg/l, ▽: 0.876 kg/l, ◇: 1.001 kg/l.

Figure 3. Solubilities of anthracene in carbon dioxide at 50°C. Squares - this study, circles - Rossling and Franck data [10].

Figure 4. Enhancement factor, C/C°, for the anthracene + CO_2 system at different temperatures: O - 40°C, □ - 60°C, Δ - 95°C.

Figure 5. Frequency shift of the maximum of the C-H band of anthracene as a function of density. Δ - data taken at 95°C, □ - 60°C and O - 40°C.

Fig. 1

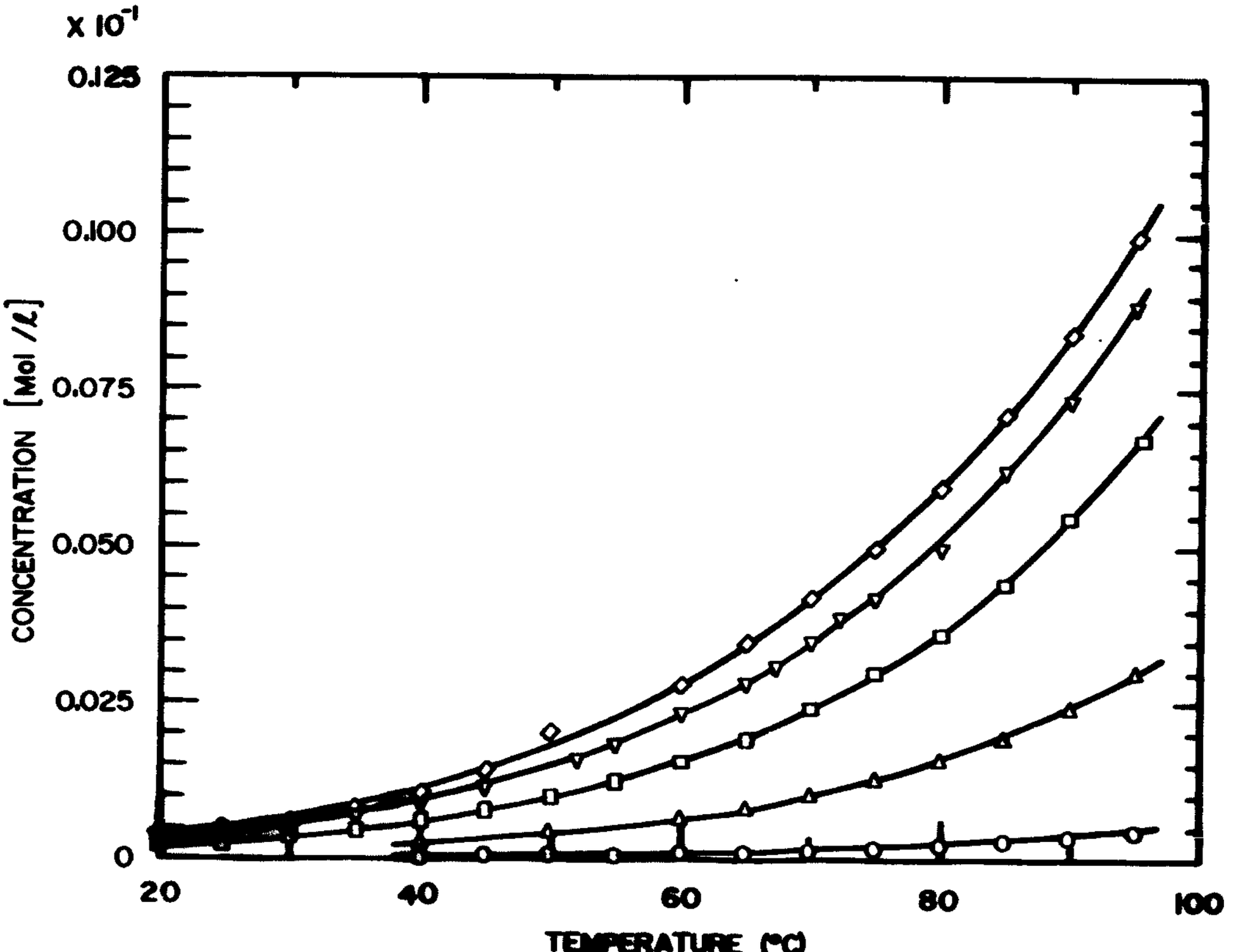
X 10⁻¹
0.125
0.100
0.075
0.050
0.025
0
CONCENTRATION [Mol /L]
20
40
60
80
100
TEMPERATURE (°C)

Fig. 2

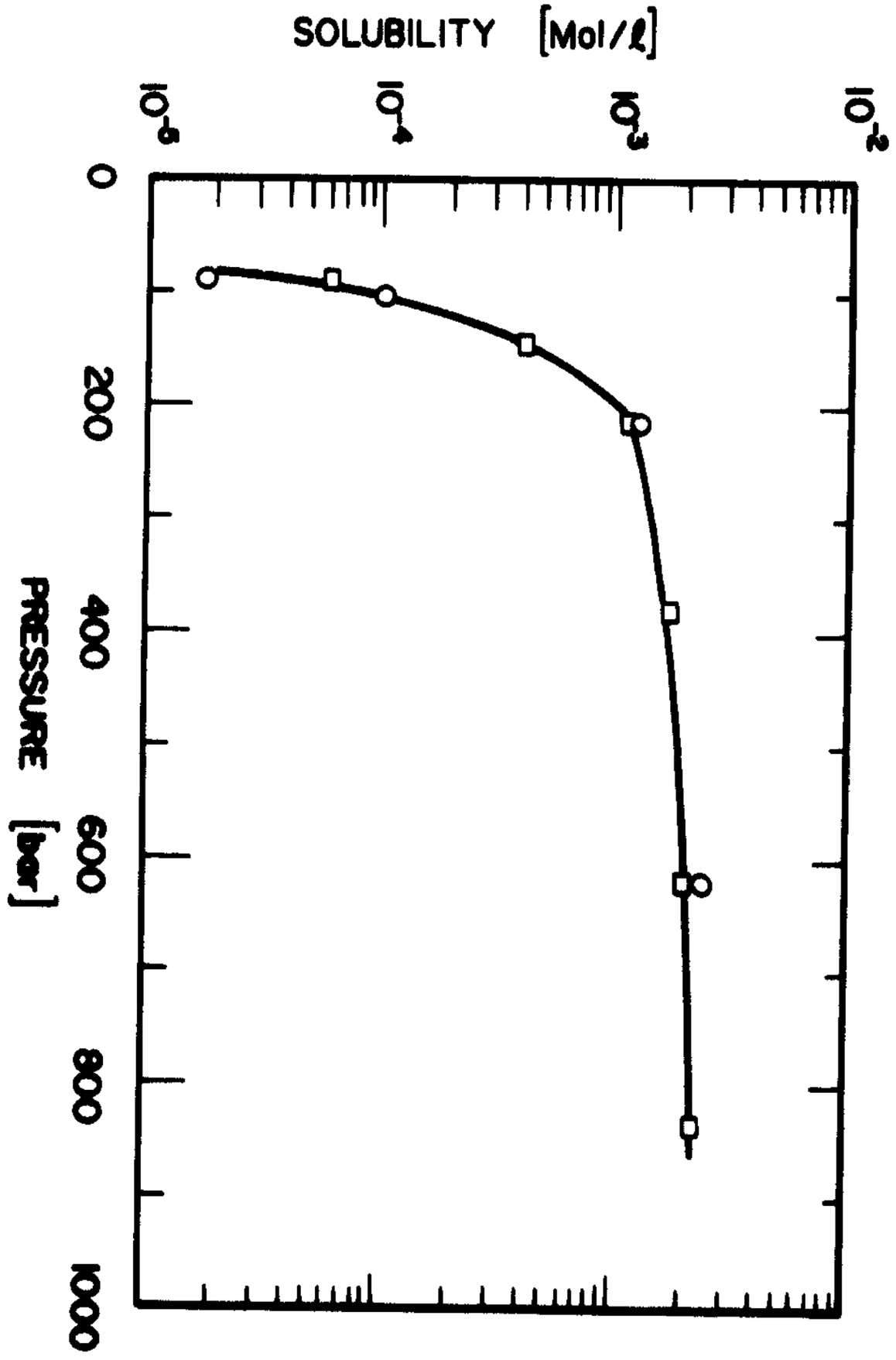
SOLUBILITY [Mol/ℓ]
10^{-5}
10^{-4}
10^{-3}
10^{-2}
0
200
400
600
800
1000
PRESSURE [bar]

Fig. 3

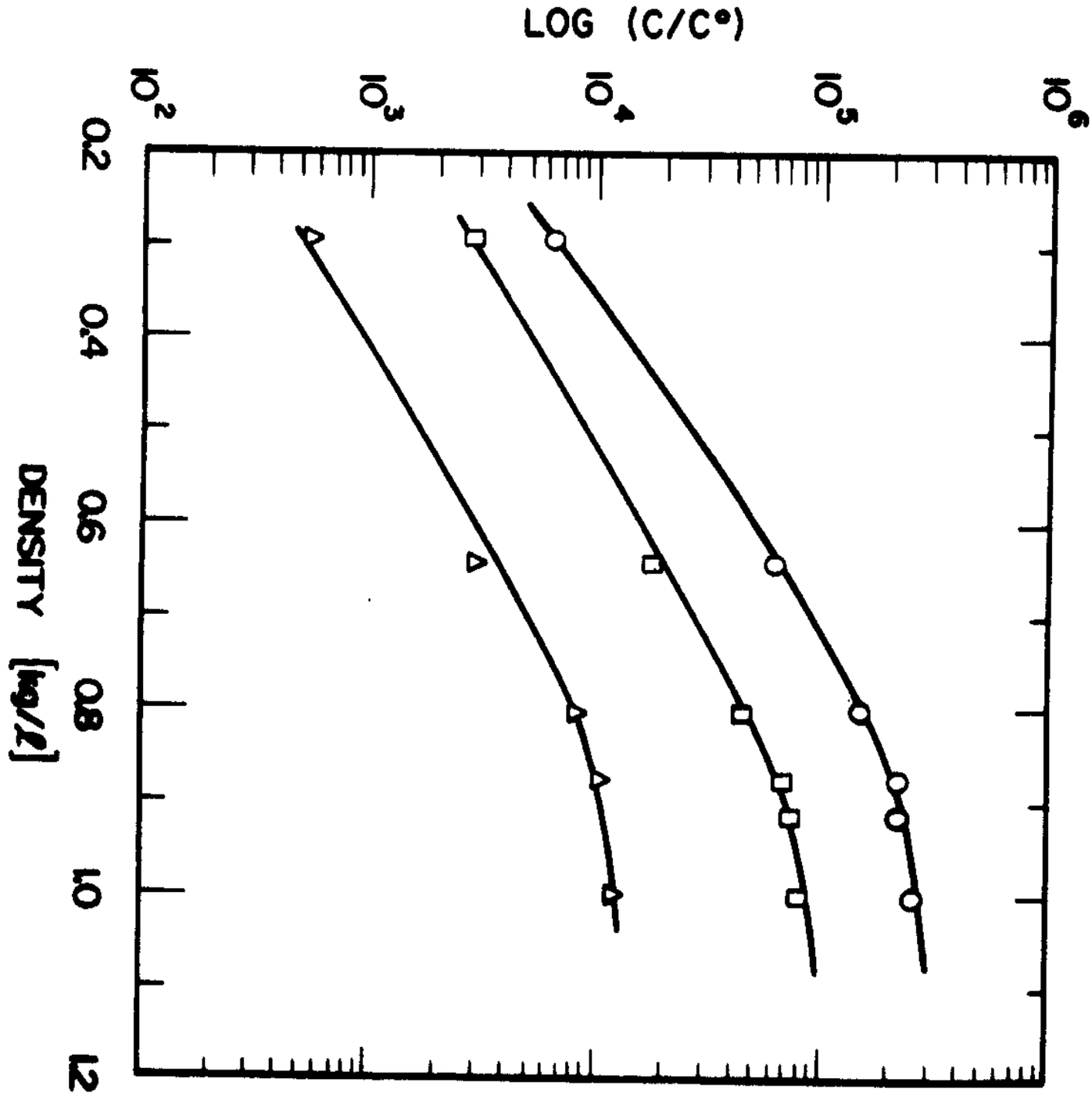

Fig. 4

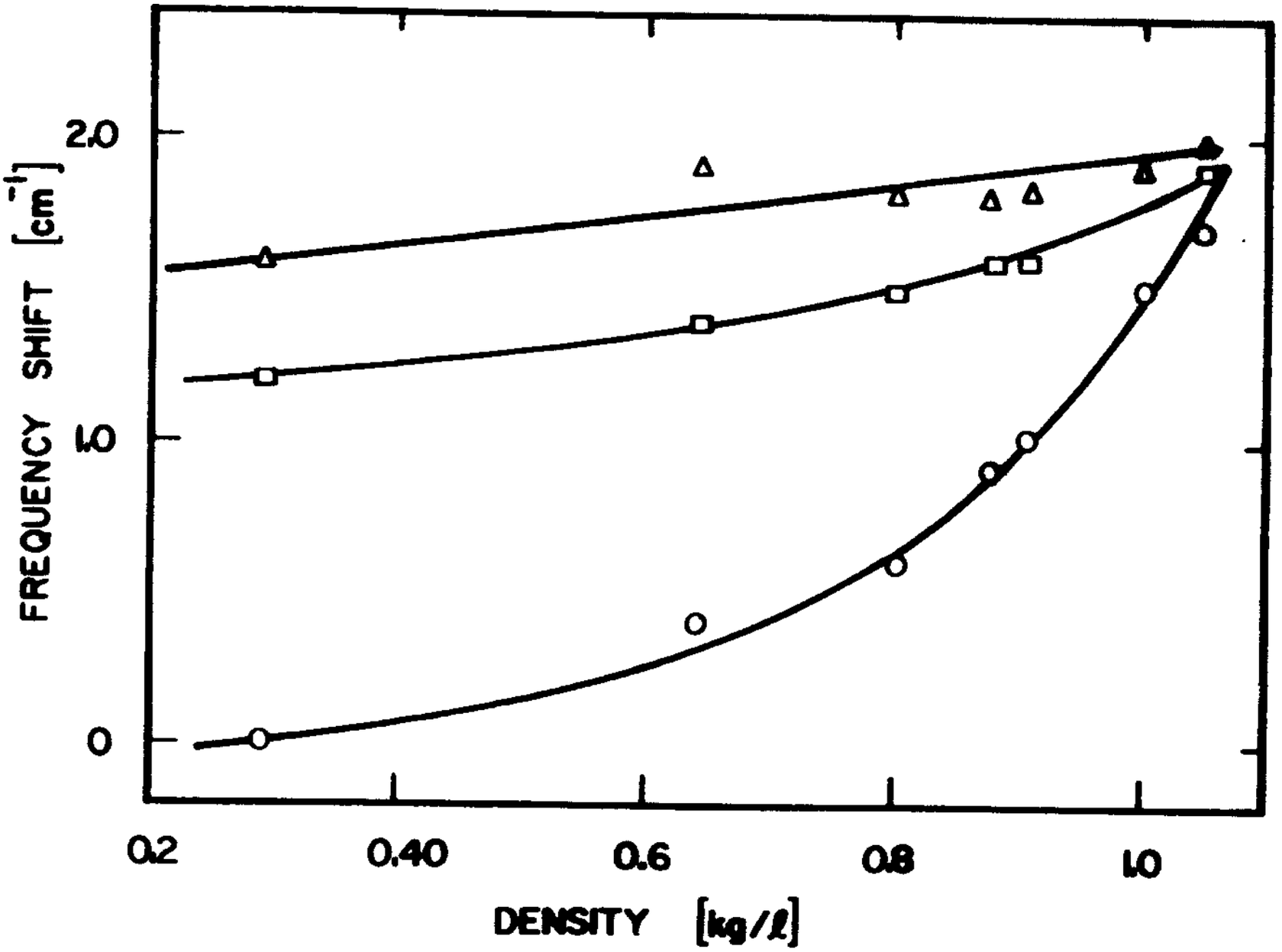

Fig. 5

Table 1. Solubilities of Anthracene in CO_2

DENSITY [kg/l^{-1}]	PRESSURE [bar]	TEMPERATURE [°C]	SOLUBILITY [mol/l^{-1}]
.294	80.4	40	$2.61_{10}-5$
	84.4	45	$5.21_{10}-5$
	89.0	50	$5.94_{10}-5$
	94.7	55	$7.44_{10}-5$
	99.8	60	$9.67_{10}-5$
	106.5	65	$1.12_{10}-4$
	113.7	70	$1.33_{10}-4$
	118.4	75	$1.64_{10}-4$
	124.0	80	$2.23_{10}-4$
	129.0	85	$2.89_{10}-4$
	132.6	90	$3.44_{10}-4$
	137.0	95	$4.44_{10}-4$
.643	100.0	40	$2.49_{10}-4$
	143.9	50	$4.06_{10}-4$
	168.8	60	$6.17_{10}-4$
	180.3	65	$7.88_{10}-4$
	194.8	70	$9.77_{10}-4$
	216.7	75	$1.23_{10}-3$
	232.3	80	$1.54_{10}-3$
	247.3	85	$1.84_{10}-3$
	267.0	90	$2.37_{10}-3$
	272.2	95	$2.95_{10}-3$

.803	69.5	20	$2.03_{10}-4$
	93.9	25	$2.55_{10}-4$
	119.7	30	$3.77_{10}-4$
	144.3	35	$4.58_{10}-4$
	168.4	40	$6.09_{10}-4$
	194.6	45	$7.67_{10}-4$
	215.0	50	$9.83_{10}-4$
	244.7	55	$1.23_{10}-3$
	275.1	60	$1.53_{10}-3$
	294.7	65	$1.91_{10}-3$
	318.2	70	$2.39_{10}-3$
	344.6	75	$2.95_{10}-3$
	372.1	80	$3.58_{10}-3$
	394.3	85	$4.36_{10}-3$
	416.7	90	$5.44_{10}-3$
	444.0	95	$6.84_{10}-3$
.8757	122.0	20	$3.26_{10}-4$
	152.0	25	$4.21_{10}-4$
	180.4	30	$5.38_{10}-4$
	212.4	35	$6.97_{10}-4$
	249.0	40	$8.89_{10}-4$
	273.4	45	$1.14_{10}-3$
	319.6	52.5	$1.77_{10}-3$
	335.0	55	$1.84_{10}-3$
	350.6	57.5	$2.10_{10}-3$

	363.2	60	$2.35_{10}-3$
	397.4	65	$2.83_{10}-3$
	413.1	67.5	$3.11_{10}-3$
	431.2	70	$3.50_{10}-3$
	444.6	72.5	$3.88_{10}-3$
	460.4	75	$4.17_{10}-3$
	493.2	80	$4.97_{10}-3$
	524.1	85	$6.21_{10}-3$
	557.9	90	$7.36_{10}-3$
	588.4	95	$8.83_{10}-3$
.9147	158.0	20	$3.43_{10}-4$
	196.4	25	$4.33_{10}-4$
	237.5	30	$5.78_{10}-4$
	268.3	35	$7.24_{10}-4$
	298.8	40	$9.18_{10}-4$
	380.0	50	$1.72_{10}-3$
	394.0	52.5	$1.83_{10}-3$
	412.0	55	$2.03_{10}-3$
	450.0	60	$2.54_{10}-3$
	483.8	65	$3.09_{10}-3$
	517.8	70	$3.75_{10}-3$
	555.5	75	$4.57_{10}-3$
	586.3	80	$5.59_{10}-3$
	627.2	85	$6.64_{10}-3$
	666.7	90	$7.89_{10}-3$

1.001	334.0	20	$3.92_{10}{}^{-4}$
	378.6	25	$4.63_{10}{}^{-4}$
	422.2	30	$5.97_{10}{}^{-4}$
	471.7	35	$7.76_{10}{}^{-4}$
	513.1	40	$1.05_{10}{}^{-3}$
	564.4	45	$1.31_{10}{}^{-3}$
	620.0	50	$1.99_{10}{}^{-3}$
	701.4	60	$2.78_{10}{}^{-3}$
	748.3	65	$3.48_{10}{}^{-3}$
	789.0	70	$4.18_{10}{}^{-3}$
	839.5	75	$4.97_{10}{}^{-3}$
	887.3	80	$5.94_{10}{}^{-3}$
	930.3	85	$7.12_{10}{}^{-3}$
	975.7	90	$8.41_{10}{}^{-3}$
	1020.5	95	$9.93_{10}{}^{-3}$
1.053	500.0	20	$6.11_{10}{}^{-4}$
	605.0	30	$9.91_{10}{}^{-4}$
	726.8	40	$1.43_{10}{}^{-3}$
	836.3	50	$2.22_{10}{}^{-3}$
	890.9	55	$2.67_{10}{}^{-3}$
	946.8	60	$3.21_{10}{}^{-3}$
	999.1	65	$3.90_{10}{}^{-3}$
	1053.2	70	$4.75_{10}{}^{-3}$
	1105.4	75	$5.71_{10}{}^{-3}$
	1156.5	80	$6.77_{10}{}^{-3}$

Table 2

Solubility of anthracene in carbon dioxide at 40°C.

(Concentration in mole fraction X 10^5)

P	C	
[bar]	Our Data	Data from Ref. 11
100	1.67	3.01
110	2.13	3.12
125	2.69	3.76
135	3.11	3.96
150	3.40	4.18
175	3.82	4.87
200	4.07	5.87

Chapter II

High Pressure Study of Hydrolysis

A. Introduction

The study of silicon containing gels has been under study recently. With their ability to form homogeneous, high quality glasses, without having to go through high temperature firing, they have proved to be quite interesting and at the same time a complex system to understand. The gelation procedure takes place in two steps, hydrolysis and condensation. In this study we will focus our interest on the hydrolysis step and the general dynamics behind the reaction.

Hydrolysis of a silicon alkoxide $Si(OR)_4$ to the monosilicic acid $Si(OH)_4$ does not occur in one step but has several intermediates. The partially hydrolyzed species $Si(OR)_3OH$, $Si(OR)_2(OH)_2$, $Si(OR)(OH)_3$ are all seen under reaction conditions where the hydrolysis time is measurable. At low pH, hydrolysis is very fast, occurring in less than a few minutes. Thus, it is difficult to be observed experimentally. However, at neutral pH's, hydrolysis is slow and can be detected by either NMR, Raman or IR techniques. Artaki, et al. [16] based on the Raman, UV, and NMR study of sol-gels with different chemical additives postulated that the hydrolysis depended upon the viscosity of the solution. In order to test this hypothesis, we monitored hydrolysis reaction as a function of pressure and pH and observed the resultant effects.

B. Experiment

The samples were prepared identically throughout the experiment with the one change being the pH of water added. A H_2O/methanol mixture was added dropwise to a solution of $Si(OCH_3)_4$ and methanol. This solution was being stirred while the addition was taking place and then stirred for an additional one to two minutes afterward. The concentrations of the species were chosen so that our final solution contained 1.6 M silicon and has a 10:1 molar ratio of water to silicon. The Raman samples were run at 27°C. Initially, the solution was placed in the cell and then the spectrum was recorded. However, since we could not completely clean the cell each time, and any particle that was left would serve as a site for nucleation and hence speed up the reaction, we used glass inserts instead. Now the sample was placed in the glass inserts with its movable piston, and this was placed in the cell. The pressurizing medium in the cell was acetonitrile. This was chosen because it did not have vibrational bands in the investigated frequency region. The data was taken at constant conditions, meaning that the cell wasn't moved after it was initially aligned, the optics were not changed and the laser power was constant. The Raman spectrometer consisted of a Spectra-Physics argon ion laser operating at 488 nm and 0.5W output power. A 1.2 cm^{-1} slit was used, and the scanning interval was equal to 2 cm^{-1}. The laser was polarized vertically with no analyzer. Spectra were recorded every 20 minutes and stored on floppy disks, which were later transferred to a VAX-11 computer where data analysis was done. The spectra themselves took 20 minutes to run, and this was our limiting factor in the experiment. It took at least 10 minutes to place the gel in the glass inserts,

the insert into the high pressure cell, and then alignment of the cell, so we could not find accurately the starting intensity of the TMOS band. The temperature was regulated by a Lauda circulator.

The viscosities of the solutions were measured at different pressures by a falling slug viscometer [17]. The densities were measured by a densitometer, described previously [18].

C. Results

The TMOS initially present in our solution reacts with water to varying degrees until it is completely hydrolyzed. Because of the different reduced masses of these partially hydrolyzed species, we can see them as distinct peaks.

$$Si(OR)_4 + n\ H_2O \rightarrow Si(OR)_{4-n}\ (OH)_n + n\ ROH$$

Typical Raman spectra recorded at different times are shown in Fig. 6. The band assignments of these spectra are given in Table 3. As the reaction proceeds, the TMOS concentration decays, while the other species first increase, but later decrease in time. This is shown in Fig. 6. Because of the special precautions that were taken, the intensity of the Raman peaks are proportional to the concentration. Fig. 7 depicts the time dependence of the TMOS concentration in sol-gel prepared at pH = 6. We can notice that hydrolysis proceeds faster by a factor of 6 when the pressure is increased from 1 to 2000 bar. In the same pressure region viscosity increases by only 30% (Table 5). This is in disagreement with the previously mentioned viscosity-hydrolysis relationship. It is worthwhile to note that viscosity appears to be volume dependent. When we measured the viscosity with the falling slug viscometer, we found differ-

ent T_{gel} values depending upon whether or not we rotated the cell. We also compared T_{gel} values to those measured from experiments done in Raman high pressure cell, and these also were different. Rate constants were calculated by measuring the slope of TMOS versus time plot at t=0. The reaction is pseudo-first order at times close to $T_{initial}$, but it deviates from first order as the partially hydrolyzed species are formed. Since hydrolysis is fast at high pressures, we have only a few points on the TMOS versus time curve; hence the error increases and the K values are less reliable. We do note, however, an increase in K as we increase pressure.

We also found no pH dependence on the rate constant. These values are shown in Table 4. Because there is a pressure dependence upon the rate constant, this allows us to calculate the activiation volume. We used the exponential approximation,

$$\ln K(\rho) = \ln K(\rho_o) + \Delta V^{\ddagger} P \qquad (1)$$

and found $\Delta V^{\ddagger} = -10$ cm^3/mol. Using the more accurate Tait function approximation,

$$K = \frac{\Delta V}{V_o} = C \log 10 \left(\frac{B + P}{B + P_o}\right) \qquad (2)$$

we found K, the compressibility to be -15 cm^3/mol. We expect the compressibility and the activation volume to be similar, and this is found. In Equation 2, B and C are found from the densities measurement that were made (Table 6).

D. Conclusion

This study showed that there is no linear dependence of hydrolysis versus viscosity. We see an increased rate of reaction with increasing pressure, although it is hard to learn a lot because of the errors in the data at higher pressures. There is no observed pH effect on the rate constant. The high pressure study allows us to find the activation volume which is -10 cm^3/mol and the compressibility factor which was found to be -15 cm^3/mol. Proposed studies will be concerned with more data acquisition at the higher pressures, so that we can have more points to see any possible pressure effects.

Table III. Band Assignments for the various species of monosilicic acid

ν (cm^{-1})	Assignment
645	$Si(OCH_3)_4$
675	$Si(OCH_3)_3OH$
695	$Si(OCH_3)_2(OH)_2$
720	$Si(OCH_3)(OH)_3$
795	Silicon Dimers
830	Silicon Network

Table IV. Rate Constants as a Function of pH's and Pressure

Pressure	pH = 4.9	pH = 6.0	pH = 7.5
1	-	.1602782	-
250	.2243120	.2244348	.2489061
500	-	.3409718	.2679715
1000	.4387539	.4530386	.3724084
2000	1.608015	.8311772	1.065282

Table V. Relative Sol-gel Viscosities

		Gelation Times (Hrs.)		
		Viscometer		
Pressure (bar)	Viscosities	(Unrotated)	(Rotated)	Raman Cell
1	1.00	17	22.0	18.0
250	-	-	-	-
500	1.09	-	9.33	15.0
1000	1.14	-	11.0	6.83
2000	1.28	-	8.0	6.33

Table VI. Sol-gel Densities

Pressure (bar)	Density
1	0.9167
500	0.9568
600	0.9712
1000	0.9946
2000	1.0312

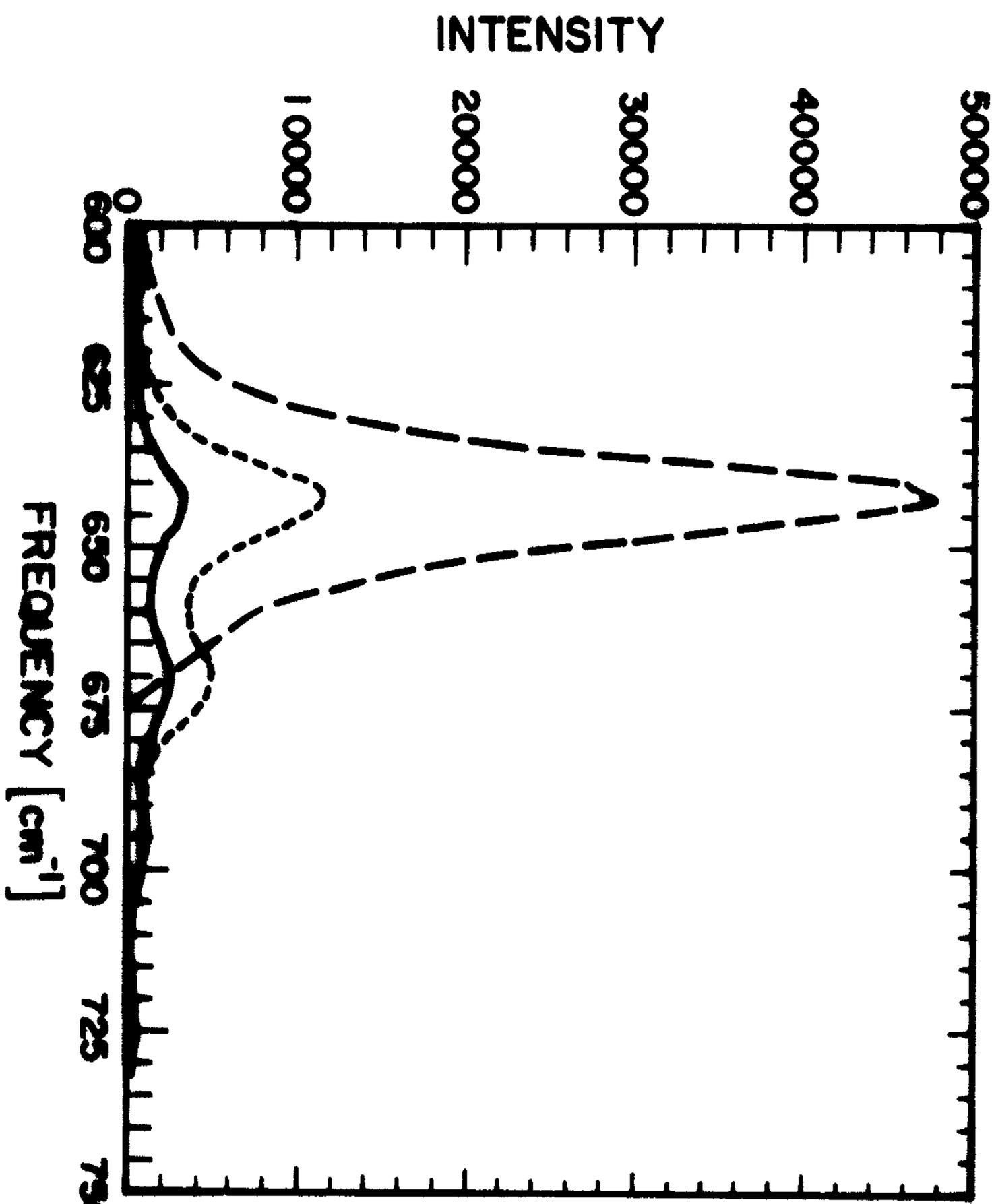

Fig. 6 Raman Spectra recorded at 250 bar (—·—: 20 min, - - - -: 4hr, ——:6hr)

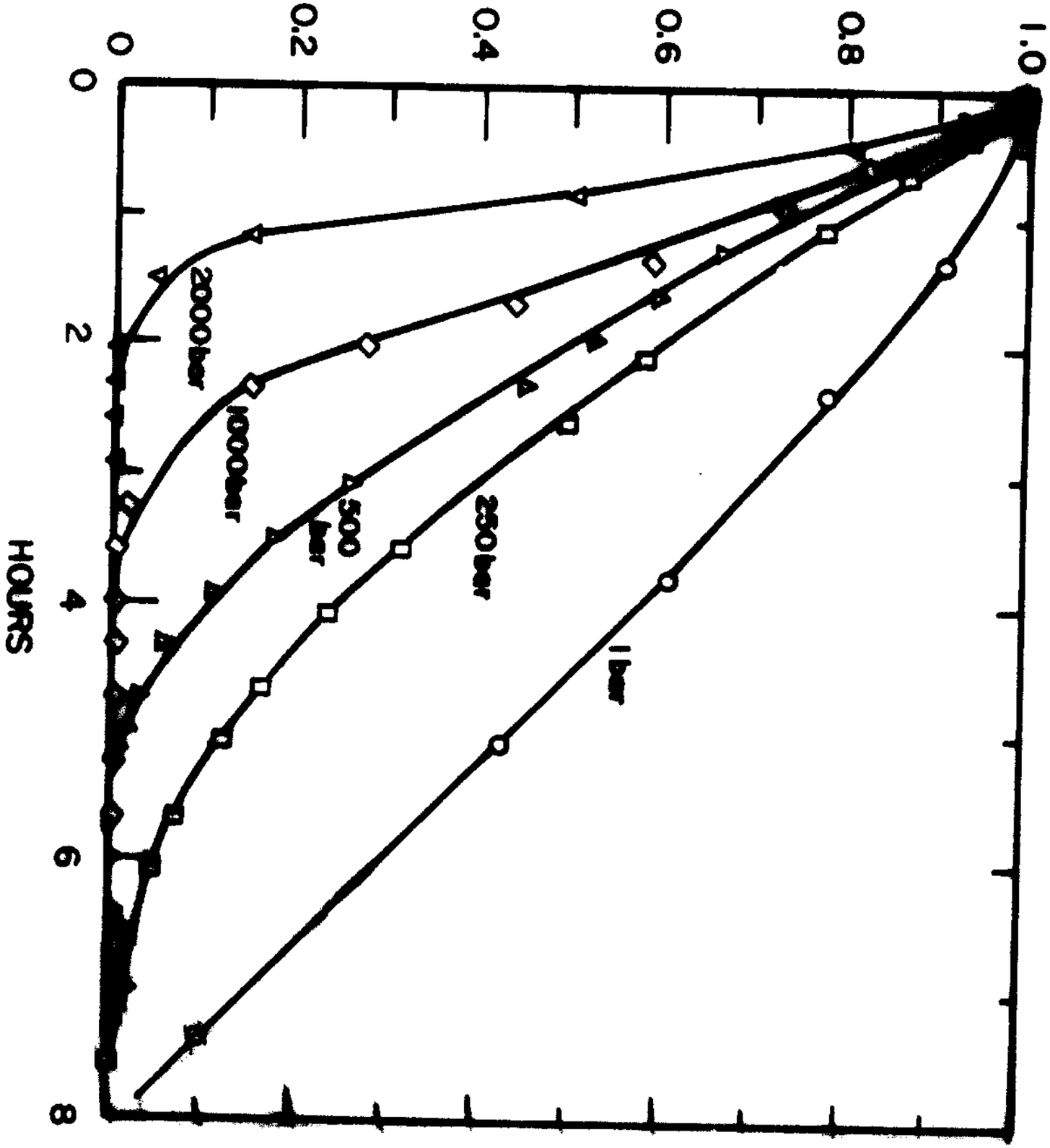

Fig. 7 Decay of TMOS as a function of time

Random Walk Model of Particle Growth

A. Introduction

As we have seen, the sol-gel system is an interesting one, but yet difficult to understand. Another approach to understand more about it, is to look at the condensation step, where the particle is being formed. Recently, there has been a lot of effort put forth to understand the process of particle growth. Computer simulations are especially well suited for this purpose, and there are numerous studies on this [19-22]. However, most of these are limited to the growth of atoms in 2 dimensions [19-22]. In this study, we attempt to simulate the growth of the gel particles in 3 dimensions with our basic interest being the complete monosilicic acid molecule. This is possible because the chemical reactions leading to the particle formation proceeds step by step and within a good approximation, we can assume that there is no correlation between two consecutive steps in the particle growth. The chemical reaction can proceed in two different steps [23].

$$\text{-Si-OH} + \text{HO-Si} \rightarrow \text{-Si-O-Si-} + H_2O \qquad (1a)$$

$$\text{-Si-OR} + \text{HO-Si} \rightarrow \text{-Si-O-Si-} + \text{ROH} \qquad (1b)$$

Each step has a different energy and probability. After the dimers are formed, the reaction continues to form trimers and longer chain molecules. At low pH, we basically have linear chains while at neutral pH's, the particle is comprised of spherical particles. Furthermore, the reaction depends upon the substituents attached to the interacting silicon atoms.

Because of the very complicated nature of the polymerization process, we will initially have to simplify it in order to simulate the particle growth. We plan various stages of simplification. At first, we will ignore completely the details of the reactions and will concentrate only on reaction 1a and the Si-O-Si bond formation in that step. Instead of taking into consideration the complete structure of the molecule of monosilicic acid and its differing structure depending upon the nature of its substituents, we will approximate interacting molecules with Si and O atoms. We will also assume that there is no correlation between consecutive steps in the polymerization process and that the probability of the reaction going to completion is constant if only geometrical configuration allows for it. In actuality, this probability is dependent, among other things, upon the angle of the incoming $Si(OH)_4$. This will be dealt with in a later stage of the simulation. This means we will not be concerned with the energy of reaction. The length of the Si-O bond is assumed constant. All these assumptions allow us to use the random walk model for the purpose of particle growth simulations. The details of this technique along with the results will be described later.

In the next step, we plan to simulate simultaneously the growth of several particles with the possibility of bond formations between these when they are close enough. This is very important, as in the real system, we have many little particles at the same time, not just one big particle.

Finally, we plan to take into account the energy of reaction, which determines the probability of forming new Si-O-Si bonds. At present, we are not aware of any studies on the energy of Si-O-Si bonds, so knowing the energy of the reaction, we will be able to replace the random walk model by a more realistic Monte Carlo technique.

B. Numerical Procedure

Initially an SiO_4 is placed in a cube of side L. L can vary, but is usually set at 100 r, r being the Si-O bond length. The initial tetrahedron is shown in Fig. 8. Instead of moving the entire SiO_4 group, which would cause complicated algebra, including the use of Euler angles, we first move a Si^*, and later when the Si^*-O-SiO_3 bond is formed, the remaining oxygens are attached to Si^* and are placed in the correct positions. The Si^* can enter the cube from each side of the cube with the same probability, and the starting position on the wall, $R = (x_1, y_1, z_1)$, is randomly chosen.

To simulate thermal motion of Si^* we generate a vector Δr_n (Δx_n, Δy_n, Δz_n) which is added to R. If the resulting position $R_1 = R + \Delta r$ is outside the cube, we start again; otherwise a new vector Δr_n is generated, and thus the Si^* moves into a new position. This process is continued until the Si^* leaves the cube or nears an oxygen to which it

oxygen bond. To have a realistic simulation, we have to set the Si-O-Si angle which can vary between 120° and 170° with an average value 144°. We will discuss this angle later. These considerations limit Si^* to be anywhere on a circle, so another angle is chosen randomly and Si^* is set (Fig. 9). In order to put the oxygens on this Si^* atom, we have to use some trigonometric formulae that are characteristic for the tetrahedron structure. We will put only 3 oxygens on the Si^*, assuming that the 4th one is on the water molecule that is the byproduct of the reaction.

The positions of the oxygens are not completely independent, but are related to the Si-O-Si bond and the tetrahedron geometry. In such a way, we form a dimer which is illustrated in Fig. 10. The described above procedure is repeated on and on and larger and larger particles are formed. A particle containing 4 silicons is shown in Fig. 11.

This program was written in Fortran on the Cyber and then transferred to the SCS VAX because of time and memory limitations. It takes about two hours CPU time to make 1200 Si atoms and 2600 oxygen atoms in our cluster. This corresponds to an elapsed time of 10 hours. Recent attempts at optimization of this program has cut down the time by a factor of 25-30%. The figures were generated by the Spher6 program written by George Phillips.

C. Results

It is known that the angle between Si-O-Si bonds in glasses varies from 120° to 170° but with an average value of 144°, but smaller values have also been reported [24]. In sol-gels one may expect this angle to

vary in much broader limits. Indeed, when we simulated gel particles setting the angle α to 144° only linear chains were formed in which only two oxygen bridges per silica are formed. From x-ray diffraction, NMR high resolution and other techniques, we know that at basic conditions the spherical particles are being formed with a majority of silicon atoms engaged in 3 and 4 oxygen bond formation. We could simulate such a situation only when the angle α was allowed to vary from 120° to 170°.

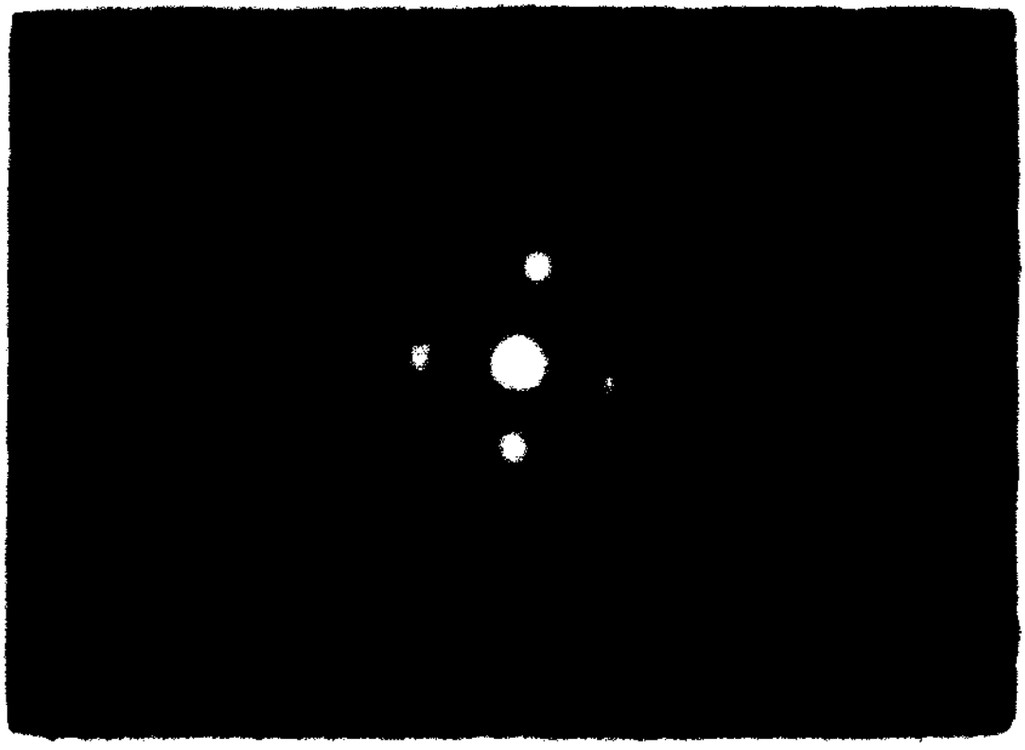

Fig. 8 Initial tetrahedron

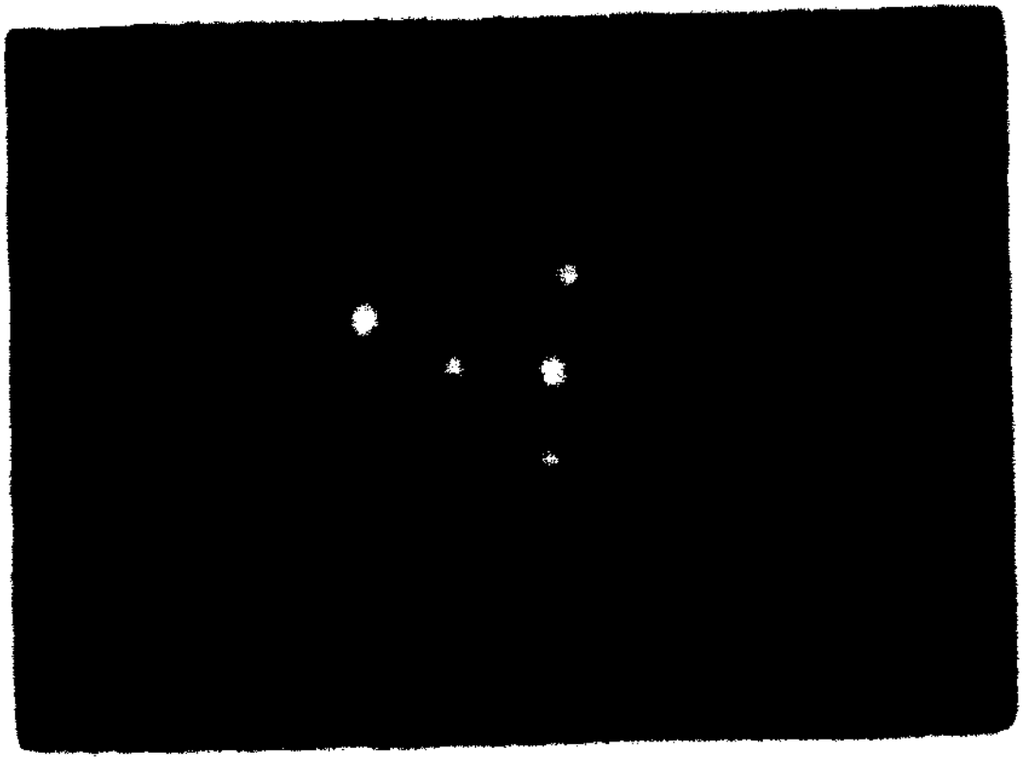

Fig. 9 Initial tetrahedron and σ_1^*

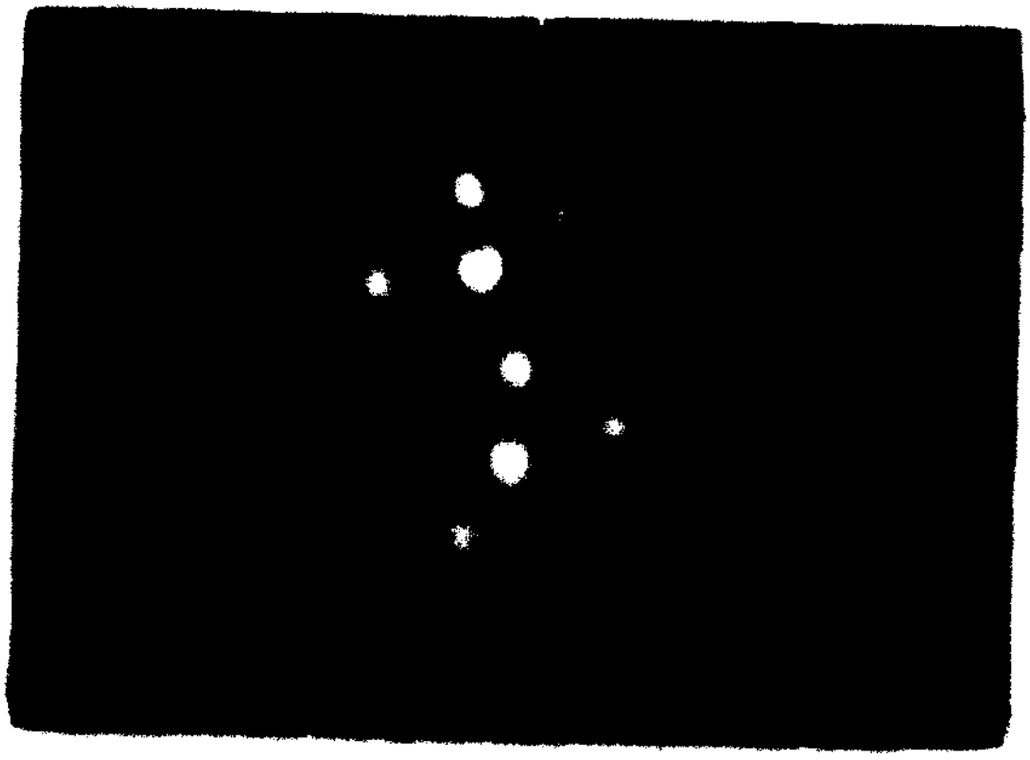

Fig. 10 Dimer

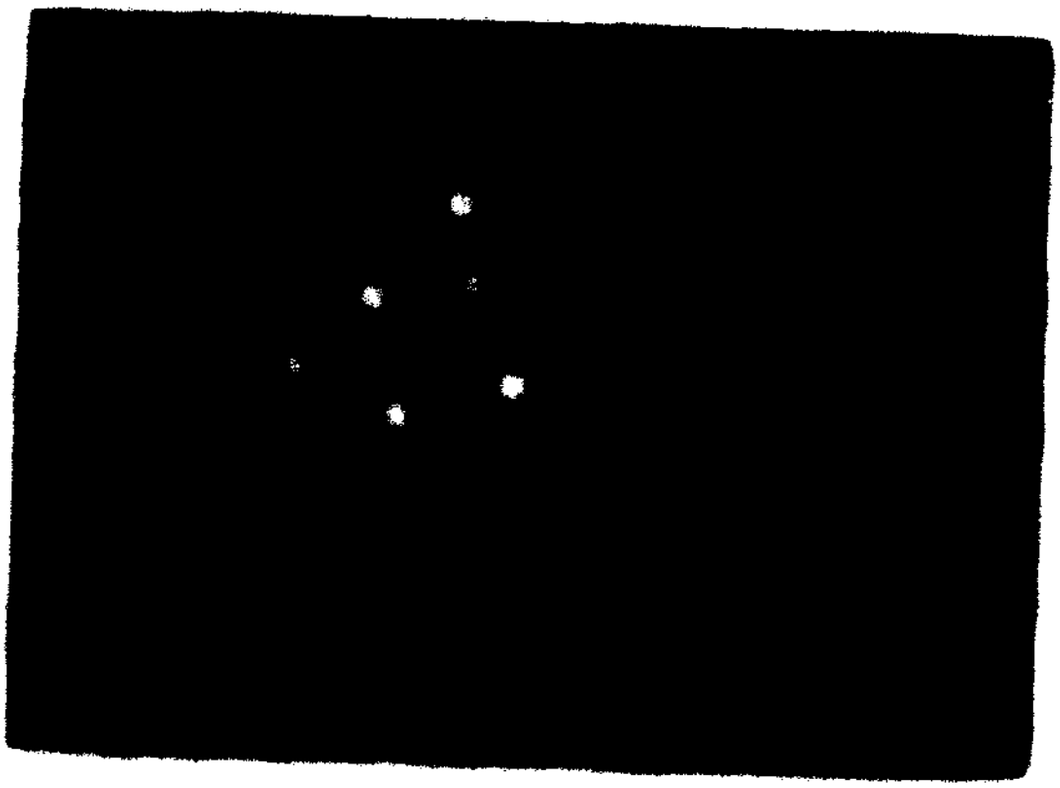

Fig. 11 Gel Particle

REFERENCES

1. O. Vitzthum and P. Hubert, German Patent 2357590, 1975.

2. M. Modell, R. P. de Fillippi and V. J. Krukonis, paper presented at the National Meeting of American Chemical Society, Miami, Florida, September 14, 1978

3. T. P. Zhuze, Petroleum 23, 298 (1960).

4. M. McHugh, M. Mallett and J. Kohn, paper presented at the Annual AIChE Meeting, New Orleans, 1981.

5. V. J. Krukonis and R. T. Kurnik, J. Chem. Eng. Data 30, 247 (1985).

6. M. E. Paulaitis, V. J. Krukonis, R. T. Kurnik and R. C. Reid, Rev. Chem. Eng. 1, 179 (1983).

7. R. T. Kurnik, S. J. Holla and R. C. Reid, J. Chem. Eng. Data 26, 47 (1981).

8. R. A. Van Leer and M. E. Paulaitis, J. Chem. Eng. Data, 25, 257 (1980).

9. J. Jonas and D. Lamb, paper presented at the ACS Symposium on Chemistry and Processing in Supercritical Fluids; at the 190th ACS National Meeting, Chicago, Il, September 9, 1985.

10. G. L. Rossling and E. U. Franck, Ber. Bunsenges. Phys. Chem. 87, 882 (1983).

11. J. Kwiatkowski, Z. Licicki and W. Majewski, Ber. Bunsenges. Phys. Chem. 88, 865 (1984).

12. T. W. Zerda, A. Hacura, J. Zerda and E. Kluk, Acta Phys. Polan. A54, 55 (1977).

13. D. M. Newitt, M.U. Pai, N. R. Kuloor and J. A. Huggill, "Thermodynamic Functions of Gases" ed. F. Din, Butterworths, London, 1962.

14. W. Schindler, T. W. Zerda and J. Jonas, J. Chem. Phys. 81, 4306 (1984).

15. K. S. Schweizer and D. Chandler, J. Chem. Phys. 76, 2296 (1982).

16. I. Artaki, M. Bradley, T. W. Zerda and J. Jonas, J. Chem. Phys. 89, 4403 (1985).

17. I. Artaki and J. Jonas, J. Chem. Phys. 82, 0000 (1985).

18. J. Akai, Ph.D. Thesis, University of Illinois, Urbana, Illinois, 1977.

19. P. Meakin and Z. R. Wasserman, Chem. Phys. 91, 391 (1984).

20. P. Meakin, Phys. Rev. A27, 1495 (1983).

21. D. A. Weitz and M. Oliveria, Phys. Rev. Lett. 52, 1433 (1984).

22. P. H. Gaskell, Disc. Farad. Soc. 50, 82 (1970).

23. I. Artaki, M. Bradley, T. W. Zerda and J. Jonas, J. Chem. Phys. 89, 4399 (1985).

24. Adrian C. Wright, J. Non-Cryst. Solids 75, 26 (1985).